Analyzing Postaliasing and Smoothing Effects of Non-separable Reconstruction Schemes on the BCC Lattice

Balázs Domonkos[1], Balázs Csébfalvi[2]

[1] Mediso Medical Imaging Systems
balazs.domonkos@mediso.hu
[2] Budapest Technology and Economics
cseb@iit.bme.hu

Abstract. Recent results demonstrate the practical advantages of the Body-Centered Cubic (BCC) lattice for regular sampling and the application of different spline filters for reconstructing an originally continuous signal from its discrete BCC-sampled representation. In order to study the frequency-domain behavior of these filters, a 3D analysis of their frequency responses is required. In our work, we apply direct volume rendering as a natural tool for such a 3D analysis. As the frequency responses are analytically known, their characteristic isosurfaces can be rendered separately in the pass band and in the stop band. The visualization of the frequency responses conveys information not just on the absolute postaliasing and oversmoothing effects, but also on their direction dependence. In this paper, we thoroughly study the frequency-domain behavior of the non-separable box splines, the non-separable DC-splines, and the tensor-product B-splines on the BCC lattice. In addition, we also analyze how the frequency responses are influenced by a discrete prefiltering, which is necessary to fully exploit the approximation power of the higher-order reconstruction filters.

1 Introduction

In volume-rendering applications, the input data is usually a discrete representation of a continuous phenomenon. In order to faithfully visualize the underlying continuous function, it has to be accurately reconstructed from its discrete samples. If the volumetric data is acquired by regular sampling on a specific lattice, the reconstruction can be easily performed by a convolution filtering. An appropriate choice of the filter kernel is of crucial importance as it directly determines the quality of the rendered images. Visual artifacts are often introduced because of the imperfect frequency-domain behavior of the applied filter [18]. Theoretically, an ideal low-pass filter can perfectly reconstruct a band-limited signal if it is sampled above the Nyquist limit [22]. The Fourier transform of such an ideal filter is a characteristic function that takes a value of one in the pass band, and a value of zero in the stop band. If the original signal is not band-limited or not sufficiently sampled, which is often the case in practice, the ideal low-pass

filter might result in ringing artifacts [18]. This prealiasing effect is caused by the drastic cut-off in the frequency domain. Ringing can be avoided by using practical filters that ensure a smooth transition between the pass band and the stop band. However, the energy of the filter in the stop band still needs to be as low as possible to reduce postaliasing effects.

For the Cartesian Cubic (CC) lattice, reconstruction filters are usually designed in 1D and extended to 3D by using a separable tensor-product extension [20, 21]. Therefore, it is sufficient to analyze the frequency-domain behavior just in 1D based on frequency plots [1, 7]. This approach, however, is not feasible for the optimal BCC lattice, since the advantageous properties of a 1D filter are not necessarily inherited in 3D if its separable extension is used on the non-separable BCC lattice. Furthermore, when a signal is sampled on a BCC lattice, its spectrum is replicated around the points of the dual Face-Centered Cubic (FCC) lattice [13], which is not separable either. Therefore, a 3D frequency-domain analysis is really necessary to study how much the aliasing spectra contribute to the reconstructed signal if a given filter kernel is applied.

The contributions of this paper are the following:

- We thoroughly analyze the frequency-domain behavior of the *box spline* [16], the *DC-spline* [12], and the *B-spline* [11] filters proposed for the BCC lattice. Previously, the frequency responses usually have been studied based on only 2D cross-sectional slices [8]. In contrast, we render the frequency responses by direct volume rendering [10]. Therefore, we can identify the preferred directions of a given filter based on the 3D distribution of its spectrum.
- We validate the results of our 3D frequency-domain analysis by rendering an appropriate BCC-sampled test signal [18]. We demonstrate that the postaliasing effect is indeed minimal along the preferred directions identified in the rendered frequency responses.
- We confirm that on the BCC lattice, the box splines perform better in the pass band, the B-splines ensure better stop-band behavior, while regarding the direction dependence, DC-splines make a compromise between the box spline and the B-spline filters. For the sake of fair comparison, we use recently proposed discrete prefilters for quasi-interpolation [8, 12, 14] that fully exploit the approximation powers of the proposed reconstruction filters.

2 Related Work

The optimal BCC lattice was first used for volume rendering by Theußl et al. [25]. However, they applied the splatting technique with spherical filters that resulted in rather blurry images. Mattausch [19] studied several practical reconstruction schemes for the BCC lattice, but the results did not show unambiguously the theoretical benefits of BCC sampling. For example, the sheared trilinear interpolation led to an anisotropic reconstruction.

The first reconstruction filters that are tailored to the geometry of the BCC lattice were proposed by Entezari et al. [13, 16]. Their non-separable *linear and*

quintic box splines provide the same approximation orders on the BCC lattice as the trilinear and tricubic B-splines on the CC lattice, respectively. Theoretically, the computational complexity of a box spline is lower than that of an equivalent B-spline, since its support is more compact and its total polynomial degree is lower. Nevertheless, this theoretical advantage cannot be exploited on the current GPUs [17], which are rather optimized for separable filtering.

Another family of non-separable filters is represented by the *BCC-splines* [6] that generalize the Hex-splines [26] for the BCC lattice. The Hex-splines were originally proposed for the hexagonal lattice, which is optimal for sampling circularly band-limited 2D signals. The BCC-splines were evaluated by a discrete approximation and their efficient piecewise formulas are not known yet.

Csébfalvi recommended a prefiltered *Gaussian reconstruction scheme* [5] adapting the principle of *generalized interpolation* [2] to the BCC lattice. This method was extended also to the *B-spline family of filters* [11]. Both the non-separable box spline filters and the tensor-product B-spline filters have been applied for quasi-interpolation on the BCC lattice [8, 14]. From a practical point of view, a separable B-spline filtering can be implemented on the recent GPUs more efficiently than a non-separable box spline filtering of the same approximation order [8, 17], since the B-splines can utilize the hardware-accelerated trilinear texture fetching [23].

Recently, Domonkos et al. [12] proposed a *discrete/continuous filter family* generated by the impulse response of the BCC trilinear kernel [19, 24]. This technique is theoretically equivalent to the discrete upsampling of the BCC-sampled volume on a higher resolution CC lattice, where the standard trilinear interpolation is used for resampling. In practice, however, the missing CC samples are calculated on the fly and not in a preprocessing. Similarly to the box spline, B-spline, and BCC-spline families, the impulse response of the BCC trilinear interpolation can also be used for generating higher-order filters by consecutively convolving the impulse response with itself. Due to the associative property of the convolution operator, the impulse responses of the DC-spline family members can be factorized to a discrete filter and a continuous filter.

Although these filtering schemes have already been compared both theoretically and practically [8, 10, 12, 17] it is worthwhile to analyze their frequency-domain behavior more thoroughly. We provide a straightforward technique for a 3D frequency-domain analysis by using direct volume rendering.

3 Frequency Responses of Reconstruction Schemes for the BCC Lattice

In this section, we review the frequency responses of the non-separable box splines, the non-separable DC-splines, and the tensor-product B-splines. As these reconstruction filters are usually applied on prefiltered data values [8, 12, 17], the Fourier transforms of the discrete prefilters are also discussed. The resultant impulse response of a prefiltered reconstruction is the convolution of the continuous reconstruction filter φ and the discrete prefilter p. Consequently, the resultant

frequency response is $\hat{\varphi}(\boldsymbol{\omega}) \cdot \hat{p}(\boldsymbol{\omega})$, where $\hat{\varphi}$ and $\hat{p}$ are the Fourier transforms of φ and p, respectively.

3.1 Box Spline Reconstruction on the BCC Lattice

The linear box spline for the BCC lattice [16] is defined by convolving a 1D box filter with itself along directions $\boldsymbol{\xi}_k$ that are defined as

$$\boldsymbol{\Xi} = [\boldsymbol{\xi}_1, \boldsymbol{\xi}_2, \boldsymbol{\xi}_3, \boldsymbol{\xi}_4] = \frac{1}{2}\begin{bmatrix} 1 & -1 & -1 & 1 \\ -1 & 1 & -1 & 1 \\ -1 & -1 & 1 & 1 \end{bmatrix}. \tag{1}$$

Since the Fourier transform of a 1D box filter is a *sinc* function, and consecutive convolutions in the spatial domain correspond to consecutive multiplications in the frequency domain, the Fourier transform $\hat{M}_{\boldsymbol{\Xi}}$ of the four-directional linear box spline $M_{\boldsymbol{\Xi}}$ is expressed as a product of four *sinc* terms [16]:

$$\hat{M}_{\boldsymbol{\Xi}}(\boldsymbol{\omega}) = \prod_{k=1}^{4} sinc(\boldsymbol{\xi}_k^T \boldsymbol{\omega}), \tag{2}$$

where $sinc(t) = \frac{sin(t/2)}{t/2}$. The quintic box spline $M_{\boldsymbol{\Xi}^2}$ is obtained by convolving the linear box spline with itself; therefore, its Fourier transform is the square of $\hat{M}_{\boldsymbol{\Xi}}(\boldsymbol{\omega})$.

To fully exploit the approximation power of the box splines, they need to be combined with discrete prefilters. Applying the framework of Condat and Van De Ville [4], Csébfalvi derived an optimal discrete prefilter [8] for a quasi-interpolating linear box spline reconstruction. The Fourier transform of this prefilter $p_{M_{\boldsymbol{\Xi}}}$ is

$$\hat{p}_{M_{\boldsymbol{\Xi}}}(\boldsymbol{\omega}) = \frac{4}{3} - \frac{1}{12}\sum_{k=1}^{4} cos(\boldsymbol{\xi}_k^T \boldsymbol{\omega}). \tag{3}$$

The quintic box spline is not an interpolating filter, but it can be combined with a discrete prefilter $p_{M_{\boldsymbol{\Xi}^2}}$ that makes it interpolating [2, 9, 17]. The Fourier transform of this prefilter [8] is $\hat{p}_{M_{\boldsymbol{\Xi}^2}}(\boldsymbol{\omega}) = 1/\hat{s}(\boldsymbol{\omega})$, where

$$\hat{s}(\boldsymbol{\omega}) = \frac{2}{5} + \frac{1}{10}\sum_{k=1}^{4} cos(\boldsymbol{\xi}_k^T \boldsymbol{\omega}) + \frac{1}{15}[cos(\omega_x) + cos(\omega_y) + cos(\omega_z)], \tag{4}$$

and $\boldsymbol{\omega} = [\omega_x, \omega_y, \omega_z]^T$. Note that the prefiltering is, in fact, a deconvolution that is performed as a division by $\hat{s}$ in the frequency domain.

3.2 DC-Spline Reconstruction on the BCC Lattice

The BCC lattice can be obtained from a CC lattice such that all CC lattice points are removed where the discrete coordinates i, j, and k are neither all even

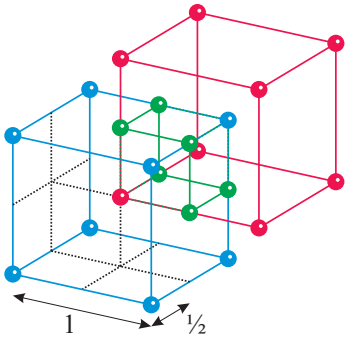

Fig. 1. Trilinear interpolation on the BCC lattice: The BCC lattice points are located on the interleaved red and blue CC lattices. The green samples are interpolated from two BCC samples of the same color. Inside the green cubic cell a standard trilinear interpolation is applied.

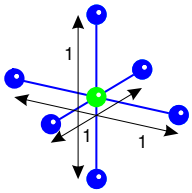

Fig. 2. The discrete components of the trilinear filter for the BCC lattice. The green sample has the value of one while the blue samples have the value of half. This discrete filter is responsible for producing the missing CC samples in an upsampled CC representation.

nor all odd numbers. The BCC trilinear interpolation reproduces these "missing CC samples" by interpolating between the available BCC samples. The BCC lattice can also be interpreted as two interleaved CC lattices. Figure 1 shows two cubic cells of these interleaved CC lattices that intersect each other in a smaller cubic cell depicted in green. The green cubic cell has only two corners that are BCC lattice points, the others (the green dots) need to be interpolated from two BCC samples along either red or blue edges. Afterwards, a simple trilinear interpolation is performed inside the green cell.

The green samples are, in fact, reconstructed using a discrete filter on the BCC lattice. This filter is shown in Figure 2. The resultant impulse response χ^1_{BCC} of the BCC trilinear interpolation is obtained by convolving this discrete filter with a scaled trilinear kernel $\beta^1(2\boldsymbol{x})$:

$$\chi^1_{\mathrm{BCC}}(\boldsymbol{x}) = \beta^1(2\boldsymbol{x}) + \frac{1}{2}\sum_{k=1}^{6}\beta^1(2(\boldsymbol{x}-\boldsymbol{v}_k)), \tag{5}$$

where

$$[\boldsymbol{v}_1,\boldsymbol{v}_2,\boldsymbol{v}_3,\boldsymbol{v}_4,\boldsymbol{v}_5,\boldsymbol{v}_6] = \frac{1}{2}\begin{bmatrix} 1 & -1 & 0 & 0 & 0 & 0 \\ 0 & 0 & 1 & -1 & 0 & 0 \\ 0 & 0 & 0 & 0 & 1 & -1 \end{bmatrix}.$$

Since χ^1_{BCC} is constructed as a convolution of a discrete filter and a continuous filter, its Fourier transform $\hat{\chi}^1_{\mathrm{BCC}}$ is easy to derive by multiplying the Fourier

transforms of these two components:

$$\hat{\chi}^1_{\mathrm{BCC}}(\boldsymbol{\omega}) = \left[1 + cos\left(\frac{\omega_x}{2}\right) + cos\left(\frac{\omega_y}{2}\right) + cos\left(\frac{\omega_z}{2}\right)\right] \hat{\beta}^1\left(\frac{\boldsymbol{\omega}}{2}\right), \tag{6}$$

where $\boldsymbol{\omega} = [\omega_x, \omega_y, \omega_z]^T$. The linear DC-spline filter χ^1_{BCC} is interpolating and also quasi-interpolating of order two by using a discrete prefilter [8, 12]:

$$\hat{p}_{\chi^1_{BCC}}(\boldsymbol{\omega}) = \frac{17}{12} - \frac{5}{48}\sum_{k=1}^{4} cos(\boldsymbol{\xi}_k^T \boldsymbol{\omega}). \tag{7}$$

Similarly to other spline families of filters, the impulse response χ^1_{BCC} of the BCC trilinear interpolation can also be used for generating higher-order filters by consecutively convolving χ^1_{BCC} with itself [12]. Thus the cubic DC-spline χ^3_{BCC} is defined as:

$$\hat{\chi}^3_{\mathrm{BCC}}(\boldsymbol{\omega}) = \hat{\chi}^1_{\mathrm{BCC}}(\boldsymbol{\omega}) \cdot \hat{\chi}^1_{\mathrm{BCC}}(\boldsymbol{\omega}). \tag{8}$$

The cubic DC-spline is non-interpolating; therefore a discrete prefiltering for generalized interpolation is necessary to use it for interpolation [2, 8, 9, 12]. The Fourier transform of this prefilter is $\hat{p}_{\chi^3_{BCC}}(\boldsymbol{\omega}) = 1/\hat{s}(\boldsymbol{\omega})$, where

$$\hat{s}(\boldsymbol{\omega}) = \frac{1}{54}\Big[\frac{35}{2} + 5c_{0,0,2} + \frac{157}{32}(c_{1,1,1} + c_{-1,1,1}) + \frac{1}{8}c_{-2,0,2} + \frac{1}{4}c_{0,2,2} + \frac{1}{32}(c_{1,1,3} + c_{-1,1,3} + c_{-1,-1,3})\Big] \tag{9}$$

where $c_{a,b,c} = \sum_{(i,j,k)\in \mathrm{perm}(a,b,c)} \cos(\frac{i\omega_x + j\omega_y + k\omega_z}{2})$. Additionally, the prefiltering fully exploits the approximation power of the reconstruction filter, so the prefiltered cubic DC-spline reconstruction leads to quasi-interpolation [3, 4, 9, 8] of order four, that is, it can perfectly reproduce polynomials of at most third degree.

3.3 B-Spline Reconstruction on the BCC Lattice

Although the tensor-product B-splines are not tailored directly to the geometry of the BCC lattice like the linear and quintic box splines, their application on BCC-sampled data can still be reasonable because of two reasons. First, the B-splines show very good antialiasing properties on the BCC lattice [8]. Second, a B-spline filtering can be efficiently implemented on the recent GPUs exploiting that the BCC lattice consists of two interleaved CC lattices [11]. For example, in a GPU-accelerated isosurface-rendering application, a B-spline reconstruction [8] turned out to be four to five times faster than an optimized non-separable box spline reconstruction [17] of the same approximation order.

The Fourier transform of the trilinear B-spline β^1 is

$$\hat{\beta}^1(\boldsymbol{\omega}) = [sinc(\omega_x)sinc(\omega_y)sinc(\omega_z)]^2. \tag{10}$$

Since the tricubic B-spline β^3 is the convolution of the trilinear B-spline with itself, its Fourier transform is $\hat{\beta}^3(\boldsymbol{\omega}) = \hat{\beta}^1(\boldsymbol{\omega}) \cdot \hat{\beta}^1(\boldsymbol{\omega})$.

To better fit the frequency response of the trilinear B-spline filter to the geometry of the dual FCC lattice, an optimal discrete prefilter of Finite Impulse Response (FIR) has been proposed [8], which guarantees a quasi-interpolation of order two. The Fourier transform of this prefilter is

$$\hat{p}_{\beta^1}(\boldsymbol{\omega}) = \frac{5}{3} - \frac{1}{6} \sum_{k=1}^{4} cos(\boldsymbol{\xi}_k^T \boldsymbol{\omega}). \tag{11}$$

Similarly to the trilinear B-spline, the tricubic B-spline cannot be used for interpolation on the BCC lattice either. Instead, it is suitable for quasi-interpolation of order four if it is combined with a discrete prefilter p_{β^3} of Infinite Impulse Response (IIR) [8]. Interestingly, the Fourier transform of this prefilter is the square of $\hat{p}_{M_{\mathbf{\Xi}^2}}$. Thus, for a quasi-interpolating tricubic B-spline reconstruction, the same prefilter is used as for the interpolating quintic box spline reconstruction, but the prefiltering is performed twice.

4 3D Frequency-Domain Analysis

Having the analytical frequency response of a reconstruction filter known, its oversmoothing and postaliasing effects can be analyzed. Marschner and Lobb defined error metrics [18] for oversmoothing and postaliasing as the squared deviation from the ideal pass-band and stop-band behavior, respectively. However, in 3D, these error metrics express only the absolute measures of oversmoothing and postaliasing effects, and do not tell anything about their direction dependence or 3D distribution. Therefore, a 3D analysis is necessary to better understand the frequency-domain behavior of a filter, especially if it is non-separable or applied on a non-separable lattice. Since, in case of BCC sampling, the spectrum of the original signal is replicated in the frequency domain around the dual FCC lattice points, the shape of the pass band is a rhombic dodecahedron [13], which is the Voronoi cell of the FCC lattice (see Figure 3). To analyze the oversmoothing effect, it has to be visualized how much the frequency response of the applied reconstruction filter differs from that of the ideal low-pass filter in the pass band. Consequently, the postaliasing effect is analyzed by visualizing the frequency response in the stop band. Here the energy of the filter should be as low as possible to well approximate the ideal low-pass filter. Furthermore, it is worthwhile to emphasize those frequency components that are closer to the centers of the aliasing spectra, since mostly these components contribute to the postaliasing effect. For this purpose, we will use an appropriate penalty function.

Direct volume rendering is a natural tool for visualizing an analytically known 3D frequency response. Note that the preferred directions of the spectrum can be identified in 3D more easily than in cross-sectional 2D slices [8]. Nevertheless, the behavior of the filter in the pass band and in the stop band cannot be separated. First, we tried to render the spectrum using different colors inside and outside the

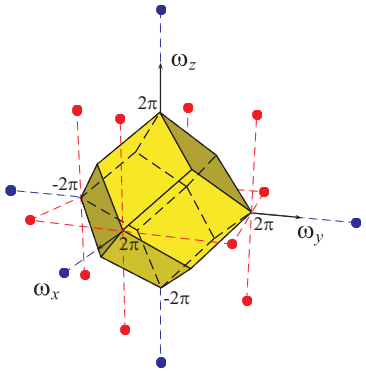

Fig. 3. The pass band corresponding to BCC sampling is the Voronoi cell of the dual FCC lattice, which is a rhombic dodecahedron. The red dots depict the first nearest neighbors, whereas the blue dots depict the second nearest neighbors.

Filter	approx. order	vanishing moments 1st	vanishing moments 2nd
linear box spline	2	2	4
quintic box spline	4	4	8
linear DC-spline	2	2	2
cubic DC-spline	4	4	4
trilinear B-spline	2	4	2
tricubic B-spline	4	8	4

Fig. 4. Approximation orders and the number of vanishing moments (the order of zero crossings) of different spline filters at the nearest and second nearest lattice points in the dual FCC lattice points.

pass band. This approach, however, was not informative when the filter had high energy in the stop band, since in this case the pass band often became almost completely hidden. Therefore, we decided to separately render the spectrum in the pass band and in the stop band. This is favorable regarding also the transfer function specification, which requires different parameter tuning for analyzing the oversmoothing and postaliasing effects.

4.1 Postaliasing

In order to visualize the stop-band behavior, we used a two-step opacity transfer function $t(r(\hat{\varphi}))$. Function r, which maps a frequency response $\hat{\varphi}(\boldsymbol{\omega})$ to $r(\hat{\varphi}(\boldsymbol{\omega})) = |\hat{\varphi}(\boldsymbol{\omega})|^{\frac{1}{6}}$, is responsible for making even the low-intensity parts of the spectrum visible. Function t, which enhances a characteristic isosurface of the frequency response, is defined as follows:

$$t(r) = \begin{cases} \frac{1}{2}[1-(1-2r)^{\frac{1}{8}}] & \text{if } 0 \le r \le \frac{1}{2} \\ \frac{1}{2}[1+(2r-1)^{\frac{1}{8}}] & \text{if } \frac{1}{2} < r \le 1. \end{cases} \tag{12}$$

To emphasize the aliasing frequencies especially in the vicinity of the dual FCC lattice points, we used the following penalty function:

$$w(\boldsymbol{\omega}) = \left(\frac{1}{2} + \frac{1}{8}\sum_{k=1}^{4} cos(\boldsymbol{\xi}_k^T \boldsymbol{\omega})\right)^2. \tag{13}$$

Note that w is periodic on the FCC lattice and takes its maximum at the lattice points. Getting far from the lattice points, w is monotonically decreasing.

Figure 5 shows the frequency responses in the stop band weighted by w. The images show the interval $[-4\pi, 4\pi]^3$ in the frequency domain. The pass band is depicted as an opaque rhombic dodecahedron. The red dots represent the twelve first nearest neighbors, whereas the blue dots depict the six second nearest neighbors. Note that the images are ordered according to the overall postaliasing effects of the corresponding reconstruction filters. The linear box spline results in the highest total postaliasing, whereas the tricubic B-spline leads to the lowest total postaliasing. Concerning the direction dependence, the box splines introduce higher aliasing frequencies along the diagonal directions, while the postaliasing effect of the B-splines is the strongest along the major axes. Representing a compromise between the box splines and the B-splines, the DC-splines suppress these aliasing frequencies isotropically. Note that, generally, a discrete prefiltering increases the total postaliasing effect but does not change the preferred directions that are mostly determined by the reconstruction filter itself.

The Fourier transform of a BCC-sampled signal contains the replicas of the primary spectrum around the points of the dual FCC lattice. Therefore, the FCC lattice points except the origin represent the "DC" components of the aliasing spectra, which mostly contribute to the postaliasing effect. If the frequency response of the filter is significantly non-zero at these lattice points, a *sample-frequency ripple* [18] might occur.

Although both the box splines, the DC-splines, and the B-splines ensure zero-crossings at the centers of the aliasing spectra [16, 8], they do not suppress the aliasing frequencies in the vicinity of the centers uniformly along different directions (see Figure 4). This can lead to direction-dependent postaliasing called *near-sample-frequency ripple* [18]. Theoretically, the order of the zero-crossings (in other words, the number of *vanishing moments* [16]) expresses how much the aliasing spectra are suppressed around the dual FCC lattice points. At the nearest twelve FCC lattice points (see the red dots in Figure 3), which are located along the diagonal directions at $[\pm 2\pi, \pm 2\pi, 0]$, $[\pm 2\pi, 0, \pm 2\pi]$, and $[0, \pm 2\pi, \pm 2\pi]$, the trilinear and tricubic B-splines ensure *four* and *eight* vanishing moments, respectively [8]. In contrast, at these points of the frequency domain, the linear and quintic box splines guarantee just the minimal number of their vanishing moments, which are *two* and *four*, respectively. As a consequence, based on the theory developed in [15], the BCC B-splines can suppress the postaliasing effect more efficiently along the diagonal directions than the non-separable box splines.

On the other hand, at the six second nearest FCC lattice points (see the blue dots in Figure 3) located along the major axes at $[\pm 4\pi, 0, 0]$, $[0, \pm 4\pi, 0]$, and $[0, 0, \pm 4\pi]$, the linear and quintic box splines ensure *four* and *eight* vanishing moments, while the trilinear and tricubic B-splines guarantee just the minimal number of their vanishing moments, which are *two* and *four*, respectively. Thus, the non-separable box splines suppress the postaliasing effect more efficiently along the major axes than the B-splines.

The linear and cubic DC-spline filters isotropically suppress the nearest aliasing spectra that contribute most to the postaliasing effect, since the orders of

their zero-crossings are *two* and *four* for both the nearest and the second nearest FCC lattice points. Thus, DC-splines perform similarly to the box splines in the diagonal directions and they perform like the B-splines along the major axes. In this sense, even if the DC-splines do not have the postaliasing frequencies of the least average magnitude, considering the direction dependence, they have the most isotropic postaliasing effect.

The rendered frequency responses of the stop band in Figure 5 completely confirm the explanation of the direction-dependent postaliasing based on the number of vanishing moments. It is clearly apparent that the box splines introduce aliasing frequencies in the directions of the twelve nearest FCC lattice points, the B-splines cause aliasing in the directions of the six second nearest FCC lattice points, while the DC-splines introduce moderate aliasing in both directions. However, as the frequency responses decay rapidly, it is favorable if the number of vanishing moments is increasing by getting closer to the origin and not vice versa. The B-splines fulfill this requirement better than the box splines and the DC-splines of the same approximation powers with and without prefiltering, since the B-splines have twice as many vanishing moments as the other filters have at the nearest FCC lattice points. Especially around the pass band, the B-splines produce the thinnest postaliasing shell.

4.2 Oversmoothing

In order to visualize the pass-band behavior, we use only the transfer function t (see Equation 12). Thus, the opacity at a frequency $\boldsymbol{\omega}$ is set to $t(|\hat{\varphi}(\boldsymbol{\omega})|)$, where $\hat{\varphi}$ is the frequency response. Furthermore, we set the opacity to zero outside the rhombic dodecahedron that represents the pass band. The border of the pass band is also depicted as an opaque rhombic dodecahedron cut in a half. Figure 6 shows the frequency responses rendered by these settings.

Note that the lowest oversmoothing is ensured by the interpolating prefiltered quintic box spline reconstruction as its frequency response almost completely fills the volume of the pass band, whereas the tricubic B-spline without prefiltering leads to the highest oversmoothing, since most of its energy is concentrated inside a sphere of a relatively small radius. On the other hand, the IIR prefiltering significantly improves the pass-band behavior of the tricubic B-spline filter.

Nevertheless, as the B-splines are not tailored directly to the geometry of the BCC lattice, even with prefiltering, they approximate the shape of the pass band with a cubic shape. In contrast, the frequency response of the interpolating prefiltered quintic box spline reconstruction nicely takes the rhombic dodecahedral shape of the pass band. DC-splines represent a transition between the box splines and the B-splines also in terms of the pass-band behavior. With and without prefiltering, the linear and cubic DC-splines perform better than the trilinear and tricubic B-splines, but they have slightly higher smoothing effect than the linear and quintic box splines. Generally, the discrete prefiltering improves the pass-band behavior of all the analyzed filters, but at the cost of a higher postaliasing (see Figure 5 for comparison).

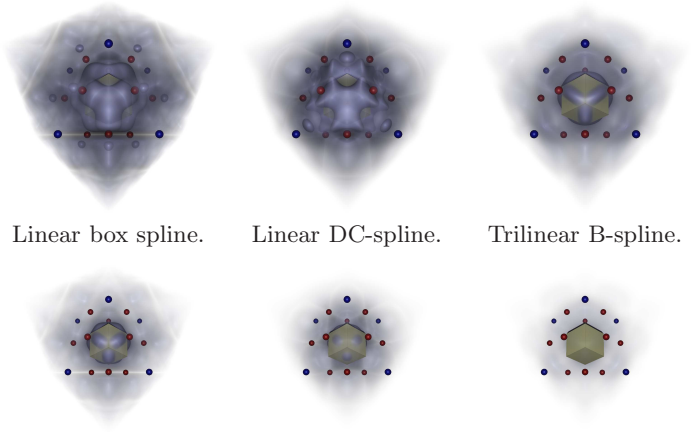

Linear box spline. Linear DC-spline. Trilinear B-spline.

Quintic box spline. Cubic DC-spline. Tricubic B-spline.

Frequency responses without prefiltering.

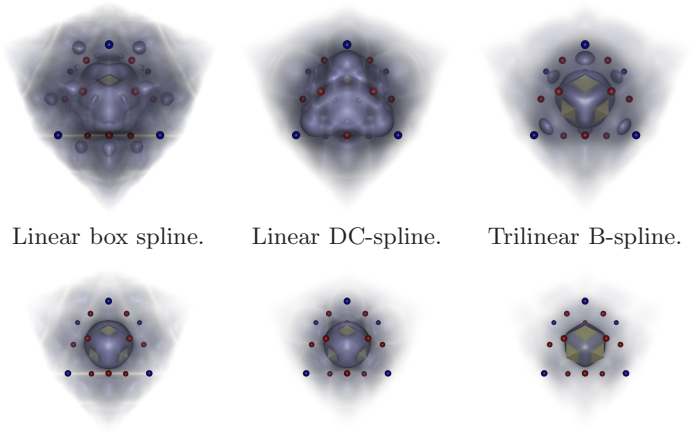

Linear box spline. Linear DC-spline. Trilinear B-spline.

Quintic box spline. Cubic DC-spline. Tricubic B-spline.

Resultant frequency responses after a discrete prefiltering.

Fig. 5. Frequency responses of different reconstruction schemes for the BCC lattice in the stop band. The penalty function w emphasizes those frequencies that are closer to the FCC lattice points. These points represent the "DC" components of the aliasing spectra, which mostly contribute to the postaliasing effect. The images show the interval $[-4\pi, 4\pi]^3$ in the frequency domain. The pass band is depicted as an opaque rhombic dodecahedron. The red dots represent the twelve first nearest neighbors, whereas the blue dots depict the six second nearest neighbors.

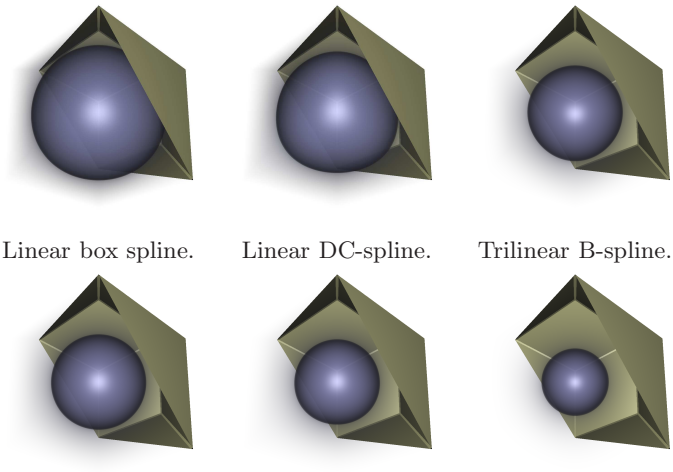

Linear box spline. Linear DC-spline. Trilinear B-spline.

Quintic box spline. Cubic DC-spline. Tricubic B-spline.

Frequency responses without prefiltering.

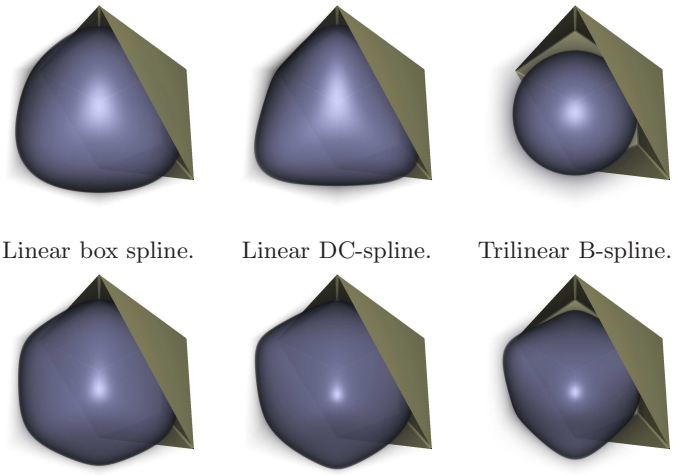

Linear box spline. Linear DC-spline. Trilinear B-spline.

Quintic box spline. Cubic DC-spline. Tricubic B-spline.

Resultant frequency responses after a discrete prefiltering.

Fig. 6. Frequency responses of different reconstruction schemes for the BCC lattice in the pass band. The images show the interval $[-2\pi, 2\pi]^3$ in the frequency domain. The opacity is set to zero outside the pass band. The border of the pass band is also depicted as an opaque rhombic dodecahedron cut in a half.

5 Experimental Results

To validate the results of our frequency-domain analysis, we rendered the isosurfaces of a well-known benchmark signal [18] using the analyzed filtering schemes. Since the linear filters cause stronger postaliasing effects than the higher-order filters, it was reasonable to apply them on a relatively oversampled volume representation. Therefore, we sampled the Marschner-Lobb signal [18] on $64^3 \times 2$ BCC lattice points. Figure 7 shows the results of quasi-interpolating prefiltered linear box spline, linear DC-spline, and trilinear B-spline reconstructions.

Note that the linear box spline produces ridge artifacts with low frequencies exactly along the diagonal directions as it has been predicted in our 3D frequency-domain analysis. Similarly, the linear DC-spline introduces moderate aliasing along both diagonal and axial directions. Furthermore, the trilinear B-spline produces aliasing with high frequencies mainly along the major axes, which also confirms our theoretical hypothesis. However, on the dual FCC lattice, the second nearest aliasing spectra along the major axes are not so closed to the primary spectrum as the first nearest aliasing spectra along the diagonal directions; therefore, the postaliasing effect of the trilinear B-spline is less apparent than that of the linear box spline and the linear DC-spline.

As the higher-order filters can better approximate the ideal low-pass filter than the linear filters, we tested them on a volume representation that samples the Marschner-Lobb signal closer to the Nyquist limit. Therefore, we took $32^3 \times 2$ BCC samples from the test signal. Figure 8 shows the results of an interpolating prefiltered quintic box spline reconstruction, an interpolating prefiltered cubic DC-spline reconstruction, and a quasi-interpolating prefiltered tricubic B-spline reconstruction. The IIR prefiltering combined with the quintic box spline and the cubic DC-spline enhances the diagonal postaliasing effects even stronger than the FIR prefiltering combined with the linear box spline and the linear DC-spline, respectively (see Figure 7). In contrast, using an IIR prefilter for a quasi-interpolating tricubic B-spline reconstruction, the circular structure of the rings can be reproduced almost perfectly without introducing direction-dependent artifacts. Although the tricubic B-spline is expected to produce high postaliasing along the major axes, the magnitude of its aliasing effect in these directions seems to be much lower than that of the quintic box spline and the cubic DC-spline along the diagonal directions.

6 Conclusion

In this paper, we have presented a comparative 3D frequency-domain analysis of reconstruction filters previously proposed for the optimal BCC lattice. According to our results, both the box splines and the B-splines cause direction-dependent postaliasing effects, but along different directions, while the DC-splines produce less direction-dependent postaliasing. The box splines maximize the postaliasing along the diagonal directions, while the B-splines produce the highest postaliasing along the major axes. However, the average magnitude of the aliasing

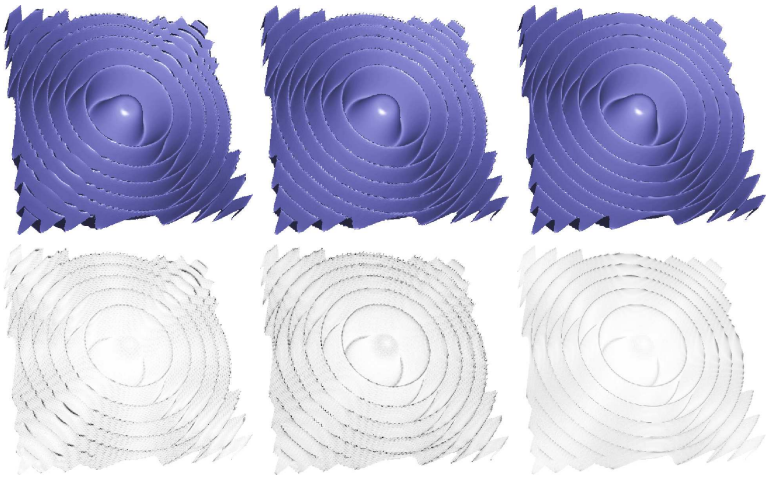

Linear box spline. Linear DC-spline. Trilinear B-spline.

Fig. 7. Quasi-interpolating prefiltered reconstruction of the Marschner-Lobb signal from $64^3 \times 2$ BCC samples using the linear box spline, the linear DC-spline, and the trilinear B-spline. The lower three images show the angular errors of the estimated gradients. Angular error of 30 degrees is mapped to black, while angular error of zero degree is mapped to white.

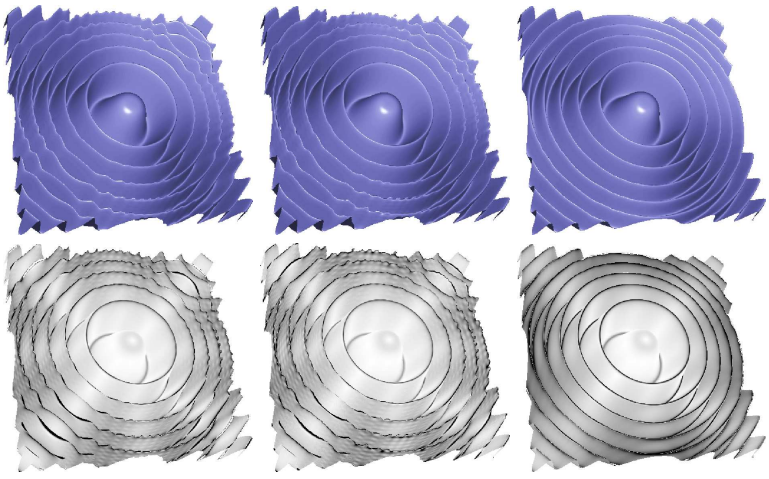

Quintic box spline. Cubic DC-spline. Tricubic B-spline.

Fig. 8. Prefiltered reconstruction of the Marschner-Lobb signal from $32^3 \times 2$ BCC samples using the interpolating quintic box spline, the interpolating cubic DC-spline, and the quasi-interpolating tricubic B-spline. The lower three images show the angular errors of the estimated gradients. Angular error of 30 degrees is mapped to black, while angular error of zero degree is mapped to white.

frequencies is the lowest in the frequency responses of the B-splines with and without prefiltering. The B-spline filters suppress especially the nearest aliasing spectra more efficiently than the box spline and the DC-spline filters. In contrast, the box splines perform best in the pass band; therefore, they can capture more high-frequency details. Particularly, the interpolating prefiltered quintic box spline reconstruction can well approximate the ideal pass-band behavior, since its frequency response almost completely fills the rhombic dodecahedral volume of the pass band. This might explain that the quintic box spline does not blur the gradients as much as the tricubic B-spline does. As a consequence, the interpolating prefiltered quintic box spline reconstruction leads to lower angular gradient error. As a compromise, the interpolating prefiltered cubic DC-spline performs better in the pass band than the quasi-interpolating tricubic B-spline but slightly worse than the interpolating prefiltered quintic box spline.

Overall, combined with the known prefilters, none of the proposed filters is superior. The advantageous properties of the box splines and the B-splines are complementary while the DC-splines can represent an appropriate compromise between them. It depends on the specific application whether the preservation of the high-frequency details or an efficient suppression of the postaliasing artifacts is considered to be more important.

Acknowledgments

This project was supported by Mediso Medical Imaging Systems, the Hungarian National Office for Research and Technology (Project ID: TECH 08/A2), and the New Hungary Development Plan (Project ID: TÁMOP-4.2.1/B-09/1/KMR-2010-0002). This work is connected to the scientific program of the "Development of quality-oriented and harmonized R+D+I strategy and functional model at BME" project.

References

1. M. J. Bentum, B. B. A. Lichtenbelt, and T. Malzbender. Frequency analysis of gradient estimators in volume rendering. *IEEE Transactions on Visualization and Computer Graphics*, 2(3):242–254, 1996.
2. T. Blu, P. Thévenaz, and M. Unser. Generalized interpolation: Higher quality at no additional cost. In *Proceedings of IEEE International Conference on Image Processing*, pages 667–671, 1999.
3. L. Condat, T. Blu, and M. Unser. Beyond interpolation: Optimal reconstruction by quasi-interpolation. In *Proceedings of the IEEE International Conference on Image Processing*, pages 33–36, 2005.
4. L. Condat and D. Van De Ville. Quasi-interpolating spline models for hexagonally-sampled data. *IEEE Transactions on Image Processing*, 16(5):1195–1206, 2007.
5. B. Csébfalvi. Prefiltered Gaussian reconstruction for high-quality rendering of volumetric data sampled on a body-centered cubic grid. In *Proceedings of IEEE Visualization*, pages 311–318, 2005.

6. B. Csébfalvi. BCC-splines: Generalization of B-splines for the body-centered cubic lattice. *Journal of WSCG*, 16(1–3):81–88, 2008.
7. B. Csébfalvi. An evaluation of prefiltered reconstruction schemes for volume rendering. *IEEE Trans. on Visualization and Comp. Graphics*, 14(2):289–301, 2008.
8. B. Csébfalvi. An evaluation of prefiltered B-spline reconstruction for quasi-interpolation on the body-centered cubic lattice. *IEEE Transactions on Visualization and Computer Graphics*, 16(3):499–512, 2010.
9. B. Csébfalvi and B. Domonkos. Pass-band optimal reconstruction on the body-centered cubic lattice. In *Proceedings of VMV*, pages 71–80, 2008.
10. B. Csébfalvi and B. Domonkos. 3D frequency-domain analysis of non-separable reconstruction schemes by using direct volume rendering. In *Proceedings of Spring Conference on Computer Graphics*, 2010.
11. B. Csébfalvi and M. Hadwiger. Prefiltered B-spline reconstruction for hardware-accelerated rendering of optimally sampled volumetric data. In *Proceedings of Vision, Modeling, and Visualization*, pages 325–332, 2006.
12. B. Domonkos and B. Csébfalvi. DC-splines: Revisiting the trilinear interpolation on the body-centered cubic lattice. In *Proceedings of VMV*, pages 275–282, 2010.
13. A. Entezari, R. Dyer, and T. Möller. Linear and cubic box splines for the body centered cubic lattice. In *Proceedings of IEEE Visualization*, pages 11–18, 2004.
14. A. Entezari, M. Mirzargar, and L. Kalantari. Quasi-interpolation on the body centered cubic lattice. *Computer Graphics Forum*, 28(3):1015–1022, 2009.
15. A. Entezari and T. Möller. Extensions of the Zwart-Powell box spline for volumetric data reconstruction on the Cartesian lattice. *IEEE Transactions on Visualization and Computer Graphics*, 12(5):1337–1344, 2006.
16. A. Entezari, D. Van De Ville, and T. Möller. Practical box splines for reconstruction on the body centered cubic lattice. *IEEE Transactions on Visualization and Computer Graphics*, 14(2):313–328, 2008.
17. B. Finkbeiner, A. Entezari, T. Möller, and D. Van De Ville. Efficient volume rendering on the body centered cubic lattice using box splines. *TR-CMPT2009-04, Graphics, Usability and Visualization laboratory, Simon Fraser Univ.*, 2009.
18. S. Marschner and R. Lobb. An evaluation of reconstruction filters for volume rendering. In *Proceedings of IEEE Visualization*, pages 100–107, 1994.
19. O. Mattausch. Practical reconstruction schemes and hardware-accelerated direct volume rendering on body-centered cubic grids. Master's thesis, TU Vienna, 2003.
20. D. Mitchell and A. Netravali. Reconstruction filters in computer graphics. In *Proceedings of SIGGRAPH*, pages 221–228, 1988.
21. T. Möller, K. Mueller, Y. Kurzion, R. Machiraju, and R. Yagel. Design of accurate and smooth filters for function and derivative reconstruction. In *Proceedings of IEEE Symposium on Volume Visualization*, pages 143–151, 1998.
22. A. V. Oppenheim and R. W. Schafer. *Discrete-Time Signal Processing*. Prentice Hall Inc., Englewood Cliffs, 2nd edition, 1989.
23. C. Sigg and M. Hadwiger. Fast third-order texture filtering. In *GPU Gems 2: Programming Techniques for High-Performance Graphics and General-Purpose Computation*, pages 313–329. Matt Pharr (ed.), Addison-Wesley, 2005.
24. T. Theußl, O. Mattausch, T. Möller, and M. E. Gröller. Reconstruction schemes for high quality raycasting of the body-centered cubic grid. *TR-186-2-02-11, Institute of Computer Graphics and Algorithms, TU Vienna University of Technology*, 2002.
25. T. Theußl, T. Möller, and M. E. Gröller. Optimal regular volume sampling. In *Proceedings of IEEE Visualization*, pages 91–98, 2001.
26. D. Van De Ville, T. Blu, and M. Unser. Hex-splines: A novel spline family for hexagonal lattices. *IEEE Transactions on Image Processing*, 13(6):758–772, 2004.